RF Field Build-up inside a Manned Space Vehicle using Novel Ray-Tracing Algorithm

Balamati Choudhury, Hema Singh, and R.M. Jha

Centre for Electromagnetics
CSIR- National Aerospace Laboratories
Bangalore- 560017, India
e-mail: balamati@nal.res.in, hemasingh@nal.res.in, jha@nal.res.in

Abstract: The radio-frequency (RF) field mapping and its analysis inside a space vehicle cabin, although of immense importance, represents a complex problem due to its inherent concavity. Further hybrid surface modeling required for such concave enclosures leads to ray proliferation, thereby making the problem computationally intractable. In this paper, space vehicle is modeled as a double-curvatured general paraboloid of revolution (GPOR) frustum, whose aft section is matched to an end-capped right circular cylinder. A 3D ray tracing package is developed that involves an uniform ray launching scheme, an intelligent scheme for ray bunching and an adaptive reception algorithm for obtaining ray path details inside the concave space vehicle. Due to non-availability of image method for concave curvatured surfaces, the proposed ray-tracing method is validated *w.r.t.* the RF field build-up inside a closed lossy cuboid using image method. The RF field build-up within the space vehicle is determined using the details of ray-paths and the material parameters. The results for RF field build-up inside a metal-backed dielectric space vehicle are compared with that of highly metallic one for parallel and perpendicular polarizations. The convergence of RF field within the vehicle is analyzed *w.r.t.* the propagation time and the number of bounces a ray undergoes before reaching the receiving point.

Keywords **-** Refined ray tracing, analytical surface modeling, RF field mapping, space vehicle

1. Introduction

In the fore section of any space vehicle, astronauts work in the presence of multiple radiating sources. This makes the astronaut cabin of space vehicle, an important indoor environment which necessitates RF field mapping. The space vehicle cabin is essentially a concave structure. Over the last decades, ray tracing has been employed for site-specific indoor propagation models [1]-[3], and it has been shown that multiple reflection is dominant for the

RF field build-up within the cavity compared to the phenomenon of diffraction [4]. Although ray tracing has been used earlier for electromagnetic (EM) analysis of aircraft cabin-like enclosures, a closer scrutiny reveals that these predominantly employ measurements to merely fit their predictions, or to validate their empirical models [5]-[7].

For EM environment analysis within the space shuttle interior (payload bay area), attempts have been made earlier to overcome the computational complexity by approximating the curved surfaces with large planar faceted plates [8]. However this leads to a completely different ray solution set, which may not necessarily approximate to the case of curvatured surfaces under consideration. Further there are sections of space vehicle, which cannot be approximated by single-curvature surfaces (e.g. circular and elliptic cylinders) and necessitate modeling with double-curvatured surfaces (e.g. spherical, paraboloidal, and ellipsoidal sections). EM analysis for convex structures, including double-curvatured structures has been done using high-frequency methods along with analytical ray tracing technique such as the *Geodesic Constant Method* (GCM) [9]. But this is restricted only to the external geometries, i.e., the convex part of such aerospace structures.

The ray tracing becomes extremely cumbersome in the important applications of crevices and concavities within an enclosure (such as space vehicles, aircraft engine, cockpit and passenger cabins) due to ray proliferation, arising from multiple reflections, transmission and diffraction. In fact the only route to ray-tracing available in such cases is *ray casting* [7], which improves the prediction only when the spatial rays are increasingly dense, leading to computational intractability. Hence a feasible ray tracing method is required to generate ray-path data for practical applications.

In the present work, a novel refined ray tracing method is developed for RF field computation inside a space vehicle including those for the microwave frequencies in the GHz region. A comprehensive 3D ray tracing package is developed in conjunction with analytical surface modeling to generate the ray path data inside a typical space vehicle. The proposed ray-tracing method is validated *w.r.t.* the RF field build-up inside a closed lossy cuboid using the image method. This is because the image method is known to be valid for planar surfaces, whereas the concave curvatured surfaces like space vehicle or aircraft in-cabin have mostly non-planar surfaces. The space vehicle is modeled as a hybrid of right circular cylinder and a general paraboloid of revolution (GPOR) frustum. The aft section is modelled by an end-capped right circular cylinder (Figure 1). The dimensions of a currently used space vehicle are considered for the RF simulations [10]. Test rays are launched from a radiating source

located inside the space vehicle and are allowed to propagate inside the space vehicle. The reflection points at each surface and the corresponding reflected rays are obtained using the parametric equation of the surface and the surface normal [9] at each incident point. As the surface parameters of the modeled space vehicle are defined through analytical equations, the ray path computation time reduced significantly.

The cumulative ray path data up to N^{th} bounce including the direct ray is used for the estimation of RF field inside a space vehicle. It includes the details of each ray-path traversed within the space vehicle before reaching the receiving point. Moreover the constitutive parameters of the space vehicle material are taken into account in calculating the total reflected power at the receiving point. It is well known that unlike the convex surfaces, the RF field mapping inside a concave structure is an extremely complex problem dominated by the proliferation of reflected ray solutions. Hence in this paper, an empty space vehicle cabin is considered to analyze the problem of concavity. The transmitting and the receiving antenna are taken as a directional antenna (half-wavelength dipole). The RF field build-up at the receiver placed within a manned space vehicle is reported for both the perpendicular and parallel polarizations. The resultant field build-up at the receiving point is obtained by a coherent summation of the fields associated with each ray reaching the receiver after undergoing multiple bounces from the walls of the space vehicle. The results are compared for a metallic space vehicle with that of a metal-backed dielectric space vehicle. The convergence of the RF field build-up is studied *w.r.t.* the propagation time and the number of reflections, a ray undergoes before reaching the receiving point.

2. Surface Modeling of a Space Vehicle

Hybrid quadratics such as general paraboloid of revolution (GPOR) frustum and finite right circular cylinder are sufficient enough to model a typical space vehicle for RF analysis. In analytical surface modeling, the surfaces are defined by parametric equations and the shaping parameters of the corresponding surfaces are calculated towards perfect matching.

A. Geometry of Space Vehicle

The schematic of the space vehicle is shown in Figure 1. The vehicle is modeled as a double-curvatured general paraboloid of revolution (GPOR) frustum, whose aft section is matched to an end-capped right circular cylinder. To describe the analytical modeling, the dimensions of a typical space vehicle considered [10] are taken as:

Length of the cylindrical body: 295.2 inch

Right circular cylinder diameter: 177.16 inch

Matched GPOR diameter: 177.16 inch

Height of GPOR frustum: 196.85 inch

B. Calculation of Shaping Parameters in Hybrid Structure

The parametric equation of right circular cylinder is given by [9]

$$x=\rho_{cyl}\cos\phi;\ y=\rho_{cyl}\sin\phi;\quad v_1 \le z \le v_2 \tag{1}$$

where, ρ_{cyl} is the radius of the right circular cylinder, ϕ is its azimuth angle that varies from 0 to 360°, and (v_2-v_1) represents the finite length of the cylinder. To model the hybrid structure, one needs to determine the shaping parameters of the structure. The parametric equation of a GPOR is given by [11]

$$x=a\ u\cos\phi;\ y=a\ u\sin\phi;\ z=-u^2 \tag{2}$$

where, ϕ is now the azimuth angle of GPOR varying from 0 to 360°, u is the GPOR basis parameter, and a is the shaping parameter that represents the sharpness/flatness of the GPOR.

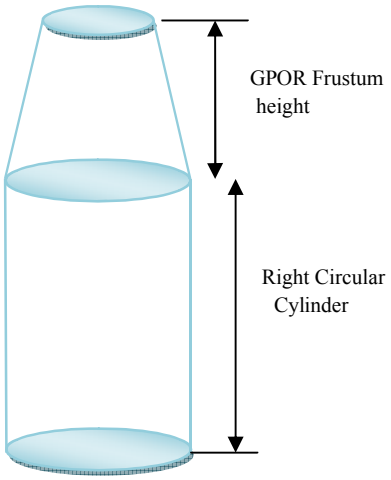

FIGURE 1: Schematic of the space vehicle.

3. Propagation inside a Space Vehicle

A novel refined ray tracing algorithm is developed for ray propagation analysis inside the concavities. The developed algorithm is validated *w.r.t* a lossy cuboid using image method as image method is not available for concave surfaces. The proposed refined ray tracing algorithm along with the RF field validation is given below.

A. Validation of Refined Ray Tracing Algorithm

As image method is simply not available for curved concavities such as the space vehicle, the RF field due to the rays obtained by the existing image method inside a lossy cuboid (2.70m×2.38m×2.40m) and those obtained by the refined ray tracing method developed in-house are compared. The RF field build up analysis is carried at 2.4 GHz. The source is kept at origin (0,0,0). The receiver is at (0.9, 1.85, 1.1). The cumulative ray paths up to 15 bounces are considered for the simulation studies. The constitutive parameters of the lossy walls of the cuboid are taken into account while estimating the net field build-up. Figure 2 presents the RF field build-up at the receiving point within the lossy cuboid (ε_r =10.74-*j*2.01, d = 4mm) for perpendicular polarization. It may be observed that the refined ray tracing algorithm has excellent agreement with image method in providing ray-path descriptions for RF field build-up within the closed cavity.

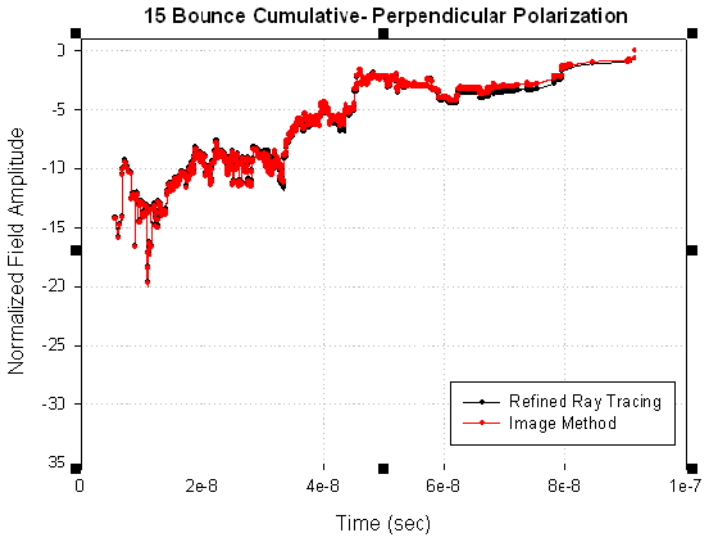

FIGURE 2: RF field build up at the receiver inside a lossy cuboid using image method and refined ray tracing method.

B. Refined Ray-Tracing inside the Space Vehicle

As described above, a closed analytically modeled hybrid space vehicle is considered for ray propagation analysis and the transmitter and receiver are located inside the space vehicle without loss of generality, at S(0.5,0.9,-15.5) and R(0.5,-0.4,-6.0). Figure 3 illustrates the schematic of the same.

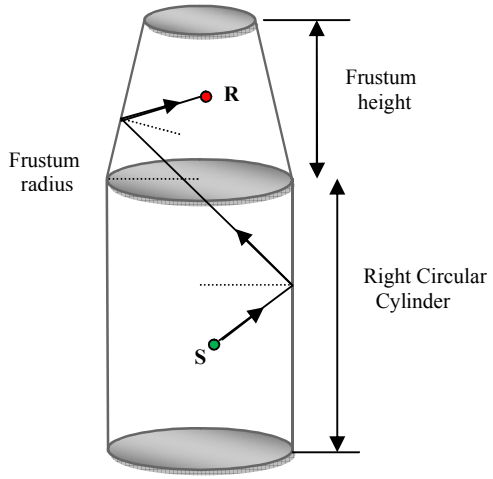

FIGURE 3: Schematic of the ray propagation inside a space vehicle.

Initially a *uniform ray launching scheme* [12] is used from the isotropic source (transmitter), which is subsequently adapted for convergence of ray solutions at the receiver. Each ray is uniquely defined by their (θ, ϕ) values. The rays are then allowed to propagate inside the cabin. The first intersection point is determined by the intersection formula between a line and the surface of the corresponding hybrid structure [13].

As the hybrid structure has four different quadratic surfaces at different heights initial intersection point is checked *w.r.t* z-coordinate and the surface equation is adopted for calculation of *first incident point.* The unit surface normal vector (Figure 4) at the first intersection point is calculated using the following equations w.r.t. the surface [9]:

The unit surface normal equation of a second degree quadric patch is given by

$$\hat{N} = x_N \hat{i} + y_N \hat{j} + z_N \hat{k} \tag{3}$$

which for a right circular cylinder is expressed as

$$x_N = \cos\phi; y_N = \sin\phi; z_N = 0; \tag{3a}$$

while for the GPOR, it is given by

$$x_N = \frac{2u\cos\phi}{\sqrt{a^2 + 4u^2}} \quad y_N = \frac{2u\sin\phi}{\sqrt{a^2 + 4u^2}} \quad z_N = \frac{a}{\sqrt{a^2 + 4u^2}} \tag{3b}$$

The unit surface normal corresponding to the above four constituent surfaces of the hybrid structure are shown in Figure 4.

Once the surface normal at the point (where the ray is incident) is determined, the reflected ray is obtained by employing the Snell's law of reflection. This process is repeated for the subsequent bounces.

An adaptive reception sphere is considered to capture the rays. The rays that reach the reception sphere are considered as the required set of rays for the RF field build-up inside the cabin. Further, an intelligent ray bunching scheme is used to avoid duplication of ray solutions.

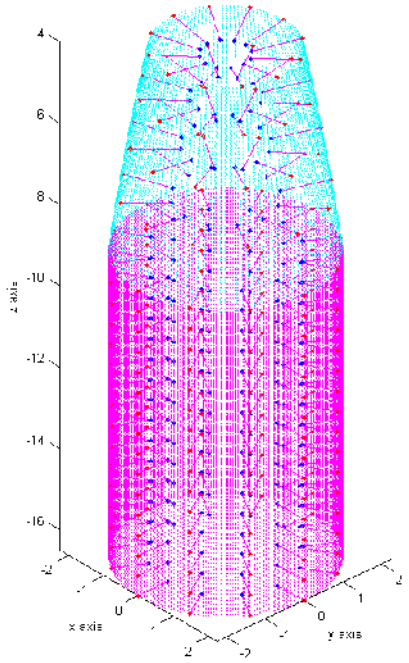

FIGURE 4: The unit surface normal vector representation of GPOR frustum and right circular cylinder.

C. Results and Visualization of Ray-path

The ray-path propagation characteristics inside the modeled space vehicle are checked for conditions of reflection, and the ray-path data up to 40 bounce (cumulative) are generated. An angular separation of 0.1^{o} is considered. It is observed that besides the *direct ray* only 66 rays reach the reception sphere cumulatively, up to 4 bounces. The ray path visualization of these 66 rays are shown in Figure 5.

The corresponding number of rays converging on to the receiver *w.r.t.* N-bounce and the program execution time is given in Table I.

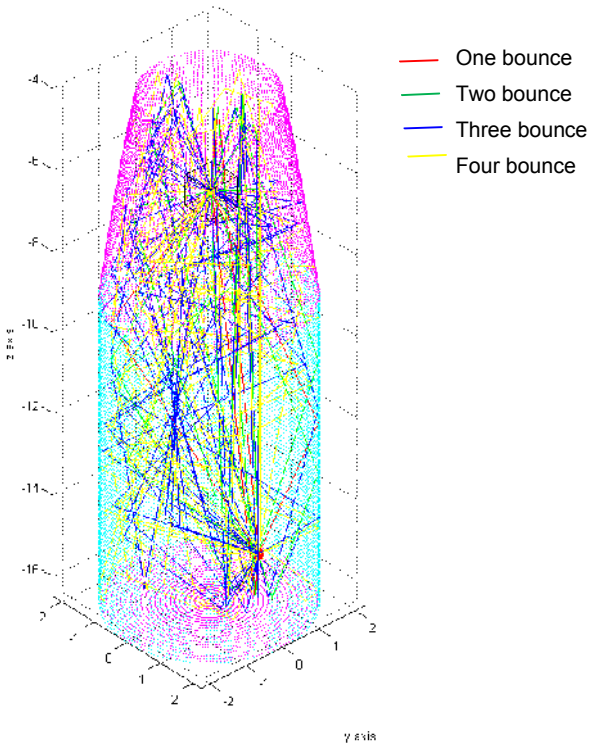

FIGURE 5. Ray-path visualization of cumulative rays up to four bounces inside the space vehicle.

It is pointed out that for the RF field mapping application under consideration, as discussed in the next section it is sufficient to consider the ray-path data up to 40 bounces.

TABLE I
Rays reaching receiver cumulatively up to N bounce and the execution time (4126183 rays are launched) in Intel Core Duo CPU; 3GHz; 4GB RAM

N-Bounce	No. of rays received	Program Execution time
1 bounce	4	25 Sec
5 bounce	120	1.55 min
10 bounce	538	6.67 min
15 bounce	893	11.00 min
20 bounce	1082	17.56 min
25 bounce	1205	24.35 min
30 bounce	1279	29.45 min
35 bounce	1318	34.12 min
40 bounce	1345	42.35 min

4. RF Field Build-up inside the Space Vehicle

RF field mapping problem is formulated in three steps, *viz*., (i) Analytical surface modeling of the space vehicle enclosure, (ii) Ray-path data generation within the enclosure using a refined ray tracing algorithm, followed by (iii) Frequency and polarization dependent EM field computation for the RF field mapping inside the space vehicle.

The RF field estimation within an enclosure needs the details of ray-paths, reflection points, radiation pattern of the transmitting and receiving antenna. In this paper, the ray-path details and the coordinates of reflection point(s) are obtained using a novel adaptive three-dimensional ray-tracing procedure, explained in the previous section. When multiple bounces and numerous ray-paths are considered, the ray tracing becomes computationally intense and complicated. However for an arbitrary concave environment, volumetric ray tracing still offers an efficient approach for RF simulation.

The resultant electric field at a receiving point P within the enclosure [14] is given by

$$E(P) = \sum_i E_i(P) \;= \sum_i E_o F_{ti} F_{ri} \left\{ \prod_l R_l \right\} e^{-jkd} L_i(d) \tag{4}$$

where $E_i(P)$ is the electric field due to the i^{th} ray at the receiver P. This ray experiences a finite number of reflections during its path from the source to the receiver. The number of the reflections a ray will undergo depends on the angle at which the ray is launched from the source.

The source is taken as a point source. The rays launched within the cavity are weighted according to the radiation pattern of the transmitting antenna. Similarly at the receiver, the rays are weighted in accordance to the radiation pattern of the receiving antenna. The time-independent field expressed in eq. (4) is the coherent sum of field contribution of individual rays reaching the receiver. The phase of each ray (reaching the receiving point at different instants of time) is adjusted accordingly. E_o is the initial field value at the source, F_{ti} and F_{ri} are the corresponding field values intercepted in the direction of ray. These field values are based on the radiation patterns of transmitting and receiving antenna, respectively. R_l is the reflection coefficient of the l^{th} interface/wall [15]-[17], d is the total ray-path length, k is the wavenumber, and $L_i(d)$ is the path loss [14]. The dependence of the reflection coefficient on the material properties, viz. permittivity, conductivity, thickness, and the angle of incidence is appropriately incorporated.

5. Results and Discussion

The RF simulations are carried out both for a metallic ($\sigma = 10^6$) space vehicle, and a metal-backed dielectric ($\varepsilon_r = 10\text{-}j5$; $d = 5$mm) space vehicle. The transmitting and receiving antennas are assumed to be directional (as half-wave dipole).

The launching of rays within an enclosure can be done efficiently for any angular separation. However, if the angular separation between the adjacent launched rays is too large, fewer test rays are launched and the RF field does not converge. This implies the requirement of launching the test rays at increasingly smaller angles, which at the other extreme is beset with the problem of computational intractability. It has been observed that a trade-off exists for the class of problems being analyzed here, optimally in the range of 0.1^o to 0.25^o. In this study, the RF field build-up at the receiving point inside a space vehicle is obtained for the ray angular separation of 0.1° launched within the space vehicle. The effect of the frequency of operation on the RF field build-up is also studied. Simulations are carried out for two distinct frequencies of 6 and 8 GHz, for both the parallel and perpendicular polarizations. It is pointed out that these distinct frequencies are commonly used in space and satellite communication applications.

First, the RF field build-up is estimated for the interior of a highly metallic space vehicle. The normalized RF field build-up at the receiving point inside the metallic space vehicle at 6 GHz is shown in Figures 6a and 6b, for the perpendicular and parallel polarization, respectively. The corresponding results at 8 GHz are given in Figures 7a and 7b, respectively. For a given ray-bounce, the complete set of rays is characterized by a distinct t_{min} and $t_{max.}$ Here t_{min} refers to the minimum time of the (shortest) ray path for a given bounce. Likewise, t_{max} corresponds to the maximum time of the (longest) ray within the set of rays for the same number of bounce. It is pointed out that for the preset number of bounce, t_{min} may be more than the propagation time of several rays of a lower bounce type, and even than some of the rays of the higher bounce type. Hence one of the focuses of this study is to analyze the RF field convergence *w.r.t.* the cumulative bounce of the feasible ray-paths (i.e., all the ray paths cumulatively up to a preset number of bounce).

In the case of perpendicular polarization (Figs. 6a and 7a), the field convergence requires very large number of bounces and hence the time axis ought to be very large. However the time window considered till 1.2 μsec, is sufficient for practical applications as shown later. The results are reported till 40-bounces (cumulative), which converges within the ambit of computational tractability.

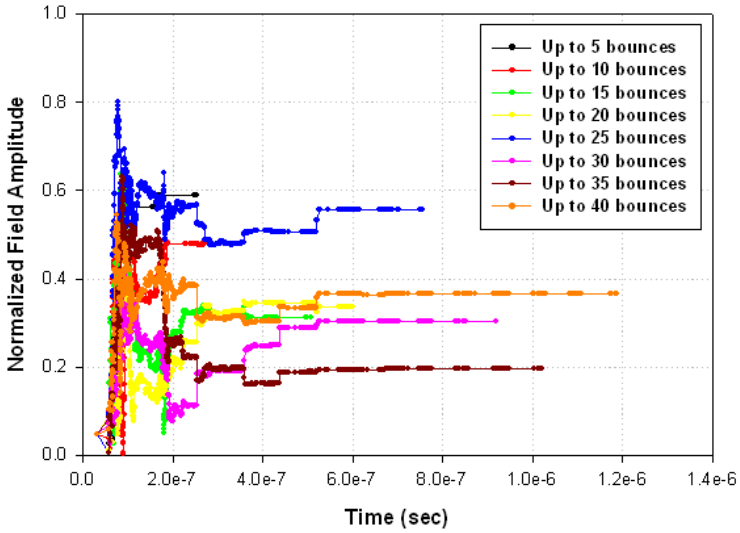

FIGURE 6a: RF field build-up inside a metallic space vehicle. Frequency = **6 GHz**; $\sigma = 1.8\times10^5$ S/m, Polarization: *Perpendicular*. Since the walls of space vehicle are metallic, convergence has not been achieved.

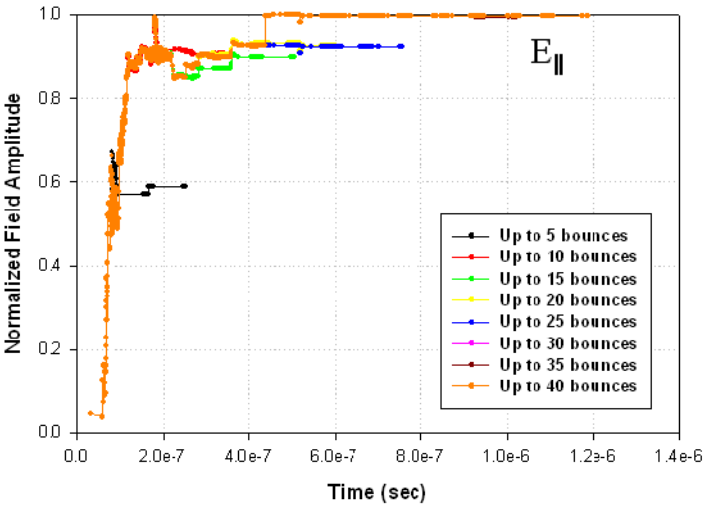

FIGURE 6b: RF field build-up inside a metallic space vehicle. Frequency = **6 GHz**; $\sigma = 1.8\times10^5$ S/m, Polarization: *Parallel*. Since the walls are metallic, convergence has not been achieved.

Since the walls of the space vehicle are considered to be highly metallic ($\sigma = 10^6$), the rays do not suffer significant attenuation at each reflection before reaching the receiver. It can be observed from Figures 6a and 7a that the level of RF field build-up for perpendicular polarization tends to broadly increase with the number of bounces considered. This is ascribed to the fact that as the number of bounces increases, the number of rays reaching the receiver also increases. These numerous rays reaching the receiver arrive from different directions, and hence tend to substantially cancel leaving only a small net (positive or

negative) RF field. This small net field contributes to the earlier threshold of the RF field build-up in the incremental sense, thereby leading to the extremely slow rate of convergence for the metallic case. This is on the expected lines since convergence has not been achieved within a highly metallic reverberation chamber like environment [18].

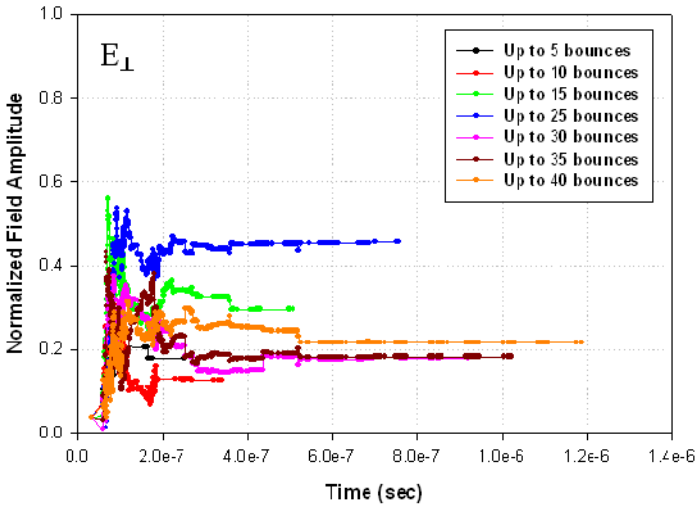

FIGURE 7a: RF field build-up inside a metallic space vehicle. Frequency = **8 GHz**; $\sigma = 1.8\times10^{5}$ S/m, Polarization: *Perpendicular*. Since the walls are metallic, convergence has not been achieved.

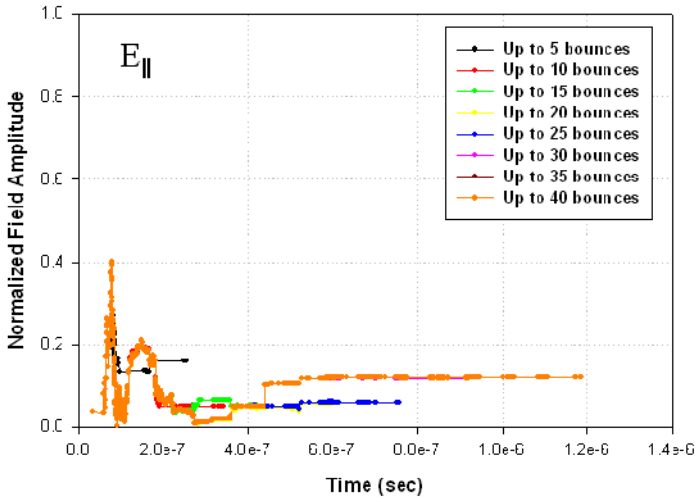

FIGURE 7b: RF field build-up inside a metallic space vehicle. Frequency = **8 GHz**; $\sigma = 1.8\times10^{5}$ S/m, Polarization: *Parallel.* Since the walls are metallic, convergence has not been achieved.

In contrast, for the parallel polarization (Figures 6b and 7b), despite of metallic walls, the RF field build-up converges rapidly. This is due to the fact that for the parallel polarization, the direction of E-field vector changes continually [17] after successive (oblique-incidence)

reflections. When the electric field associated with the multiple rays reaching the receiver are coherently superimposed, the fields with opposite phase tend to cancel each other, resulting in the rapid convergence of the total field build-up *w.r.t.* the number of bounces.

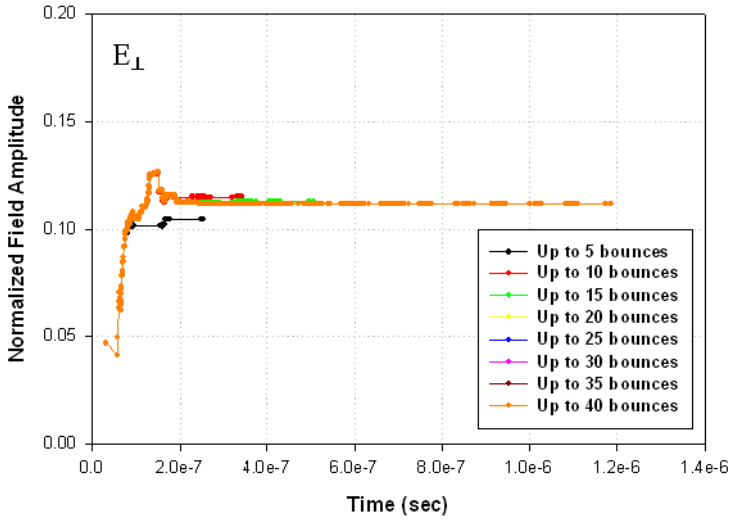

FIGURE 8a: RF field build-up inside a **metal-backed dielectric** (ε_r = 10-*j*5; d = 5mm) space vehicle. Frequency = **6 GHz**; Polarization: ***Perpendicular***. (Though the field is normalized, the y-axis considered is only up to 0.20 to facilitate closer scrutiny of the plots).

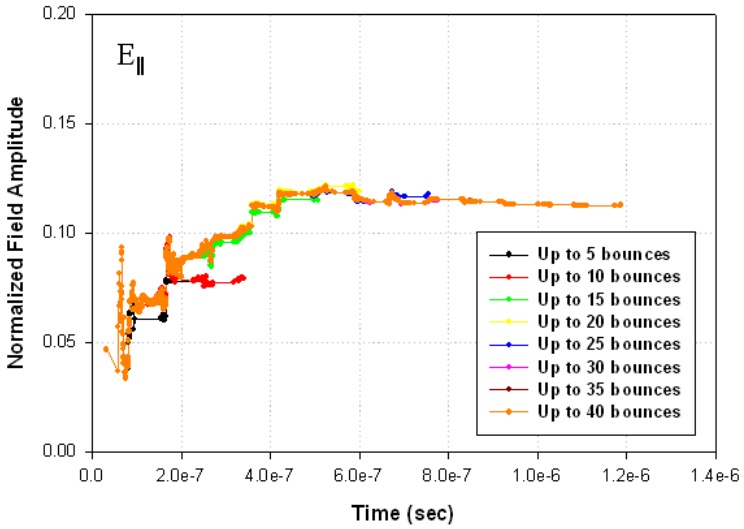

FIGURE 8b: RF field build-up inside a **metal-backed dielectric** (ε_r = 10-*j*5; d = 5mm) space vehicle. Frequency = **6 GHz**; Polarization: ***Parallel***. (Though the field is normalized, the y-axis considered is only up to 0.20 to facilitate closer scrutiny of the plots).

The amplitude of total RF field build-up at receiver, particularly initially, fluctuates with the number of bounces. This may be due to the fact that this study is emphasized *w.r.t.* the preset cumulative number of bounces, which is used as the cut-off that ignores all the higher-bounce ray paths. Although the higher bounces tend to result in increasingly diminished (and hence negligible) electric field contributions, their contribution during the initial RF build-up is not necessarily so, thereby leading to the observed RF fluctuations. However, with the increase in time, this error tends to cancel itself out.

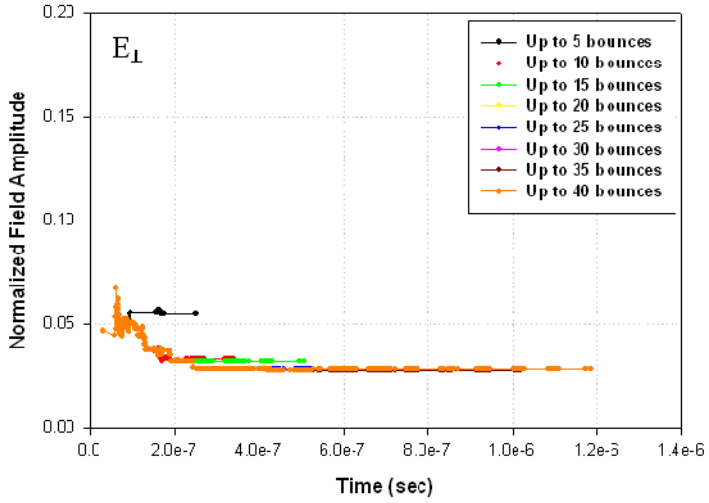

FIGURE 9a: RF field build-up inside a **metal-backed dielectric** (ε_r = 10-*j*5; d = 5mm) space vehicle. Frequency = **8 GHz**; Polarization: ***Perpendicular***. (Though the field is normalized, the y-axis considered is only up to 0.20 to facilitate closer scrutiny of the plots).

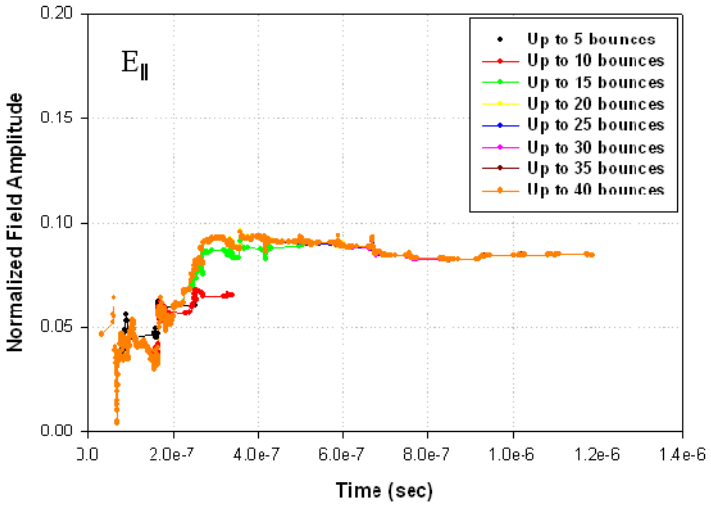

FIGURE 9b: RF field build-up inside a **metal-backed dielectric** (ε_r = 10-*j*5; d = 5mm) space vehicle. Frequency = **8 GHz**; Polarization: ***Parallel***. (Though the field is normalized, the y-axis considered is only up to 0.20 to facilitate closer scrutiny of the plots).

A discerning reader may also notice that the total RF field build-up inside a metallic space vehicle is higher at 6 GHz as compared to 8 GHz for both the polarizations. This is explained by the fact that the geometric path-length solutions (between the source and receiver points) are independent of frequency. Thus compared to 8 GHz, each ray traverses fewer electrical wavelengths over the fixed geometric path at 6 GHz, leading to lesser attenuation and hence in general higher RF field build up values.

A metal-backed dielectric space vehicle is considered next. This dielectric in reality is highly absorbent in nature. Thus a typical absorber permittivity is taken here, as $\varepsilon_r = 10\text{-}j5$; $d = 5$ mm. These constitutive parameters of the wall material are employed in the estimation of reflection coefficients [17] of each of the ray path, as a function of polarization and all the successive angles of incidence. Thus the contribution of each ray path reaching the receiver within the space vehicle can be coherently summed up after adjusting them in phase.

The resultant normalized RF field build-up within the space vehicle for 6 and 8 GHz, is shown in Figures 8 and 9, respectively. The y-axis within these field normalized plots, is limited to 0.20, to facilitate a closer scrutiny. It can be readily observed that for a metal-backed dielectric space vehicle, the ray contribution converges rapidly for both the perpendicular and parallel polarizations, both over time and the number of bounces. This is ascribed to the lossy nature of the metal-backed dielectric wall that the rays are incident upon, leading to attenuation and thus lower RF field amplitude and a rapid convergence [19].

6. Conclusion

The RF environment inside a space vehicle is analyzed based on the novel application of a refined ray-tracing algorithm proposed here along with hybrid surface modeling for the space vehicle. The refined ray tracing yields the required ray-path data, which also facilitates visualization of all the rays that reach a particular sub-cube placed inside the space vehicle cabin. A *ray-bunching* algorithm is developed to differentiate the ray solutions as ray bunches that travel nearly parallel to reach the reception sub-cube. A *refinement algorithm* is then employed to identify the ray path within this ray bunch, which eventually converges on to the receiving point.

This algorithm generates the complete data for all the ray paths cumulatively up to a given number of bounce. In the applications where higher bounces are required, denser rays need to be launched to achieve convergence, which often leads to computational intractability. In this

study, the RF field build-up at the receiving point inside a space vehicle is obtained for the rays launched at the angular separation of 0.1° within the space vehicle. Again, for the class of space vehicle cabin problem analyzed in this work, for the convergence of RF field build-up, it is sufficient to consider the ray paths cumulatively up to 40 bounces, which is within the realm of computational tractability.

The RF field build-up at the receiving point within the space vehicle is determined by summing the fields associated with each ray reaching the receiver after being adjusted in phase. The effect of operational frequency on the RF field build-up is also studied. Simulations are carried out for two distinct (uplink/downlink) frequencies of 6 and 8 GHz. The results for RF field build-up are compared for a metallic space vehicle and a metal-backed dielectric space vehicle. Since the wavelengths traversed by a ray over the fixed geometric path is a function of frequency, lower the frequency, lesser will be the number of wavelengths travelled by a ray, leading to lesser attenuation and hence higher RF field build-up values. It is due to this fact that the total RF field build-up inside a metallic space vehicle is found to be higher at 6 GHz as compared to 8 GHz for both the polarizations.

The number of rays reaching the receiver increases with the ray-bounce. These numerous rays incident from different directions tend to cancel out, leaving but a net (positive/negative) RF field. Despite the large number of rays, it is only this small net RF field that contributes to the incremental rise/ fall in the threshold of the RF field build-up. This leads to the slow rate of convergence. In the case of perpendicular polarization, the RF field build-up inside a metallic space vehicle tends to broadly increase with the number of bounces considered. This trend is on the expected lines, since it is well-known that the RF field convergence is not achieved within a highly metallic reverberation chamber. In contrast, for the parallel polarization, the direction of the E-field vector changes continually after each (oblique-incidence) reflection. When the electric field associated with the multiple rays reaching the receiver are coherently superimposed, the fields with opposite phase tend to cancel each other, resulting in the rapid convergence of the total field build-up *w.r.t.* the number of bounces.

For a metal-backed dielectric space vehicle, which is the practical case under consideration, the RF field build-up converges rapidly both *w.r.t.* the elapsed time, and the number of bounces. This is true for both parallel and perpendicular polarization. This is due to the lossy nature of metal-backed dielectric wall of the space vehicle enclosure.

References

[1] J.K. Chen, G. Veciana, and T.S. Rappaport, "Site-specific knowledge and interference measurement for improving frequency allocation in wireless networks," *IEEE Transactions on Vehicular Technology*, vol. 58, pp. 2366-2377, June 2009.

[2] K.H. Ng, E.K. Tameh, and A.R. Nix, "A new heuristic geometrical approach for finding non-coplanar multiple edge diffraction ray paths," *IEEE Transactions on Antennas and Propagation*, vol. 54, pp. 2669-2672, Sept. 2006.

[3] Y.B. Ouattara, S. Mostarshedi, E. Richalot, J. Wiart, and O. Picon, "Near- and far-field models for scattering analysis of buildings in wireless communications," *IEEE Transactions on Antennas and Propagation*, vol. 59, pp. 4229-4238, Nov. 2011.

[4] H. Suzuki and A. S. Mohan, "Measurement and prediction of high spatial resolution indoor radio channel characteristic map," *IEEE Transactions on Vehicular Technology*, vol. 49, pp. 1321-1333, July 2000.

[5] K.W. Hurst and S.W. Ellingson, "Path loss from a transmitter inside an aircraft cabin to an exterior fuselage-mounted antenna," *IEEE Transactions on Electromagnetic Compatibility*, vol. 50, pp. 504-512, Aug. 2008.

[6] N. Moraitis, P. Constantinou, F.P. Fontan, and P. Valtr, "Propagation measurements and comparison with EM techniques for in-cabin wireless networks," *EURASIP Journal on Wireless Communication and Networking,* vol. 2009, pp. 1-13, Mar. 2009.

[7] A. Kohmura, J. Picard, N. Yonemoto, and K. Yamamoto, "Measurement of EM field inside a cruising aircraft: Potential problems for the use of mobile phones on board," *Journal of Ultra-wideband, Short Pulse Electromagnetics,* vol. 9, pp. 335-342, Jan. 2010.

[8] S. U. Hwu, Y. -C. Loh, J. A. Dobbins, Q. D. Kroll, and C. C. Sham, "Space shuttle UHF communications performance," *IEEE Aerospace and Electronics Systems Magazine*, vol. 20, pp. 9-14, Oct. 2005.

[9] R.M. Jha and W. Wiesbeck, "Geodesic Constant Method: A novel approach to analytical surface-ray tracing on convex conducting bodies," *IEEE Antennas and Propagation Magazine*, vol. 37, pp. 28-38, Apr. 1995.

[10] *Jane's All the World's Aircraft* 2010-2011. P. Jackson (Ed.), Jane's Information Group, Coulsdon, UK, 1034p., ISBN 13-978-07106-2916-6, 2007-2008.

[11] L. Jossefsson and P. Persson, *Conformal Array Antenna Theory and Design*. John Wiley and Sons, ISBN 9780471465843, 512 p., 2006.

[12] S.Y. Seidel and T.S. Rappaport, "Site-specific propagation prediction for wireless in building personal communication system design," *IEEE Transactions on Vehicular Technology*, vol. 43, pp. 879-891, Nov. 1994.

[13] E. Kreyszig, *Advanced Engineering Mathematics*. 10th Edition, John Wiley, ISBN 978-04-704-5836-5, 1280 p., 2010.

[14] G. E. Athanasiadou and A. R. Nix, "A novel 3-D indoor ray-tracing propagation model: The path generator and evaluation of narrow-band and wide-band predictions," *IEEE Transactions on Vehicular Technology*, vol. 49, pp. 1152-1168, July 2000.

[15] M. Albani, G. Carluccio, and P. H. Pathak, "Uniform ray description for the PO scattering by vertices in curved surface with curvilinear edges and relatively general

boundary conditions," *IEEE Transactions on Antennas and Propagation*, vol. 59, pp. 1587-1596, May 2011.

[16] P. Russer, *Electromagnetics, Microwave Circuit and Antenna Design for Communications*. Artech House, Norwood, MA, ISBN 1-58053-532-1, 410 p., 2003.

[17] C.L. Holloway and E.F. Kuester, "Impedance-type boundary conditions for a periodic interface between a dielectric and a highly conducting medium," *IEEE Transactions on Antennas and Propagation*, vol. 48, pp. 1660-1672, Oct. 2000.

[18] D.-H. Kwon, R.J. Burkholder, and P.H. Pathak, "Ray analysis of electromagnetic field build-up and quality factor of electrically large shielded enclosures," *IEEE Transactions on Electromagnetic Compatibility*, vol. 40, pp. 19-26, Feb. 1998.

[19] Balamati Choudhury, Hema Singh, Jason P Bommer, and R. M. Jha, "RF field mapping inside large passenger aircraft cabin using refined ray-tracing algorithm," *IEEE Antennas and Propagation Magazine.* (Accepted for publication, Scheduled: Feb. 2013)